mathematics

MDPI

Article

Mathematical Model Describing the Hardening and Failure Behaviour of Aluminium Alloys: Application in Metal Shear Cutting Process

Lotfi Ben Said [1,2,*], Alia Khanfir Chabchoub [3] and Mondher Wali [2]

1 Department of Mechanical Engineering, College of Engineering, University of Ha'il, Ha'il City 2440, Saudi Arabia
2 Laboratory of Electrochemistry and Environment (LEE), National Engineering School of Sfax, University of Sfax, Sfax 5080, Tunisia
3 Higher Institute of Technological Studies of Sousse, Sousse 4023, Tunisia
* Correspondence: bensaid_rmq@yahoo.fr or lo.bensaid@uoh.edu.sa

Abstract: Recent research has focused on sheet shear cutting operations. However, little research has been conducted on bar shear cutting. The main objective of the present investigation is to study bar shear cutting with numerical and experimental analysis. Bar shear cutting is an important operation because it precedes bulk metalworking processes for instance machining, extrusion and hot forging. In comparison to sheet shear cutting, bar shear cutting needs thermomechanical modelling. The variational formulation of the model is presented to predict damage mechanics in the bar shear cutting of aluminium alloys. Coupled thermomechanical modelling is required to analyse the mechanical behaviour of bulk workpieces, in which the combined effect of strain and temperature fields is considered in the shear cutting process. For this purpose, modified hardening and damage Johnson–Cook laws are developed. Numerical results for sheet and bar shear cutting operations are presented. The comparison between numerical and experimental results of shearing force/tool displacement during sheet and bar shear cutting operations proves that the use of a thermomechanical model in the case of the bar shear cutting process is crucial to accurately predict the mechanical behaviour of aluminium alloys. The analysis of the temperature field in the metal bar shows that the temperature can reach T = 388 °C on the sheared surface. The current model accurately predicts the shear cutting process and shows a strong correlation with experimental tests. Two values of clearance (c_1 = 0.2 mm) and (c_2 = 1.2 mm) are assumed for modeling the bar shear cutting operation. It is observed that for the low shear clearance, the burr is small, the quality of the sheared surface is better, and the fractured zone is negligible.

Keywords: shear cutting; thermomechanical model; ductile fracture; Johnson–Cook model

MSC: 74R99

Citation: Ben Said, L.; Chabchoub, A.K.; Wali, M. Mathematical Model Describing the Hardening and Failure Behaviour of Aluminium Alloys: Application in Metal Shear Cutting Process. *Mathematics* **2023**, *11*, 1980. https://doi.org/10.3390/math11091980

Academic Editor: Aleksey I. Shinkevich

Received: 22 March 2023
Revised: 18 April 2023
Accepted: 21 April 2023
Published: 22 April 2023

1. Introduction

Finite element methods are increasingly being developed and used for predicting the behaviour of workpiece and tool components in manufacturing processes. Metal forming and cutting processes require knowledge of the mechanical behaviour and damage of the workpiece [1]. In fact, the accuracy of a finite element model of any metalworking process is always dependent on the robustness of the identification of the constitutive law of materials [2–4].

In decoupled models, plasticity and damage fields are independent. Various numerical models take into consideration the stress triaxiality term in damage prediction [5,6]. Others models consider the damage variable as a function of the cavity properties in porous materials [7,8]. When predicting the behaviour and ductile damage of metallic materials during cutting and forming processes, Johnson–Cook models are the most widely used laws [9,10]. Their accuracy has been proven in various works [11–14]. The Johnson–Cook plasticity law considers the thermo-plastic behaviour of workpieces in manufacturing processes with high deformation rates and high temperature variations. In addition, the Johnson–Cook damage criterion takes into account the influence of stress triaxialities on damage strain. This model was considered in computational manufacturing processes because it takes into account the high deformation rates and high temperature fields obtained in these processes, such as shear cutting and machining. The material parameters of this model are determined by experimental tests.

Recently, the shear cutting process has been widely used by mechanical industries and investigated by a larger number of numerical studies. This is due to the increasing demand for a reliable and optimal shearing process in aeronautical and automotive developments. In terms of numerical studies, the sheet shear cutting process has interested researchers more than the bar shear cutting process. Sheet and bar metalworking differ in the blank dimensions, evolution of the temperature field during cutting operations, and the anisotropy of the workpiece; each case should be studied distinctly. In this context, research works on sheet shear cutting [15–17] are more developed than those on the bar shear cutting process [18,19]. The impact of cutting parameters such as clearance and cutting speed on the quality of the sheared workpiece, shearing efficiency and tool life has been studied.

Optimization of the workpiece geometry and tool wear during shear cutting operations is a priority in the metalworking industry. Experimental and numerical studies have been performed to analyse the impact of friction, cutting speed, punch force, etc. on workpiece and cutting tools [20–22]. These studies are based on the efficiency of the computed material models, which contain hardening and damage laws. In addition, a burr deformation can frequently be illustrated in shear cutting operations on the cutting edge [23]. The burr should be deburred before the next step of manufacturing operation, such as the blanking and turning steps. Accurate shear cutting parameters have been determined for a burr-free cutting edge. A pre-shear cutting operation was studied from a numerical and experimental point of view [19]. The thermal field was not considered in the 3D numerical model. Behrens et al. [18] develop an experimental study in order to show the influence of microstructural conditions, clearance and shear rate on the shear plane quality of aluminium bars.

In recent years, researchers have studied sheet shear cutting processes with experimental and numerical investigations. However, only a few results have been determined for the bar shear cutting process. Sheet shearing studies are more advanced than bar shearing studies because of the continuous development of automobile and aeronautic fabrication. Accordingly, it is of interest that we conduct a study about the bar shear cutting process, which is an important operation that principally precedes bulk forming processes. In this paper, a mechanical and thermomechanical numerical modelling are developed. Based on experimental and numerical tests, the thermal term should be considered in plasticity and damage models to simulate the bar shear cutting process. For this purpose, a variational formulation of the thermomechanical model of shear cutting operation is developed. The efficiency of the plasticity and damage Johnson–Cook models are proved. The governing laws take into account the effect of the temperature field on the flow stress and the damage strain. Numerical tests of shear cutting operations are presented in order to prove the accuracy of the modified Johnson–Cook models in predicting ductile damage. The numerical results of sheet and bar shearing operations are presented in this paper. The comparison between the numerical and experimental results of the shear force/tool displacement, during the shearing operations of plates and bars, proves that the use of the thermomechanical model in the case of the bar shearing process is essential to flawlessly predict the behaviour of aluminium materials. In fact, the temperature field influences mechanical properties such as hardening, ductility and strain damage. The effect of shear clearance is investigated in order to emphasize the effect of this parameter on burr formation, the quality of the sheared surface and the dimensions of the fractured zone.

2. Materials and Methods

The experiments are carried out using specific shearing tools (Figure 1). The experimental cutting tests are conducted using a universal tensile machine (Figure 1a). Shear cutting tests are carried out with a constant cutting speed and at ambient temperature. Figure 1b,c show the 3D design of the employed shearing tools, which are used to cut aluminium sheets and round bars, respectively.

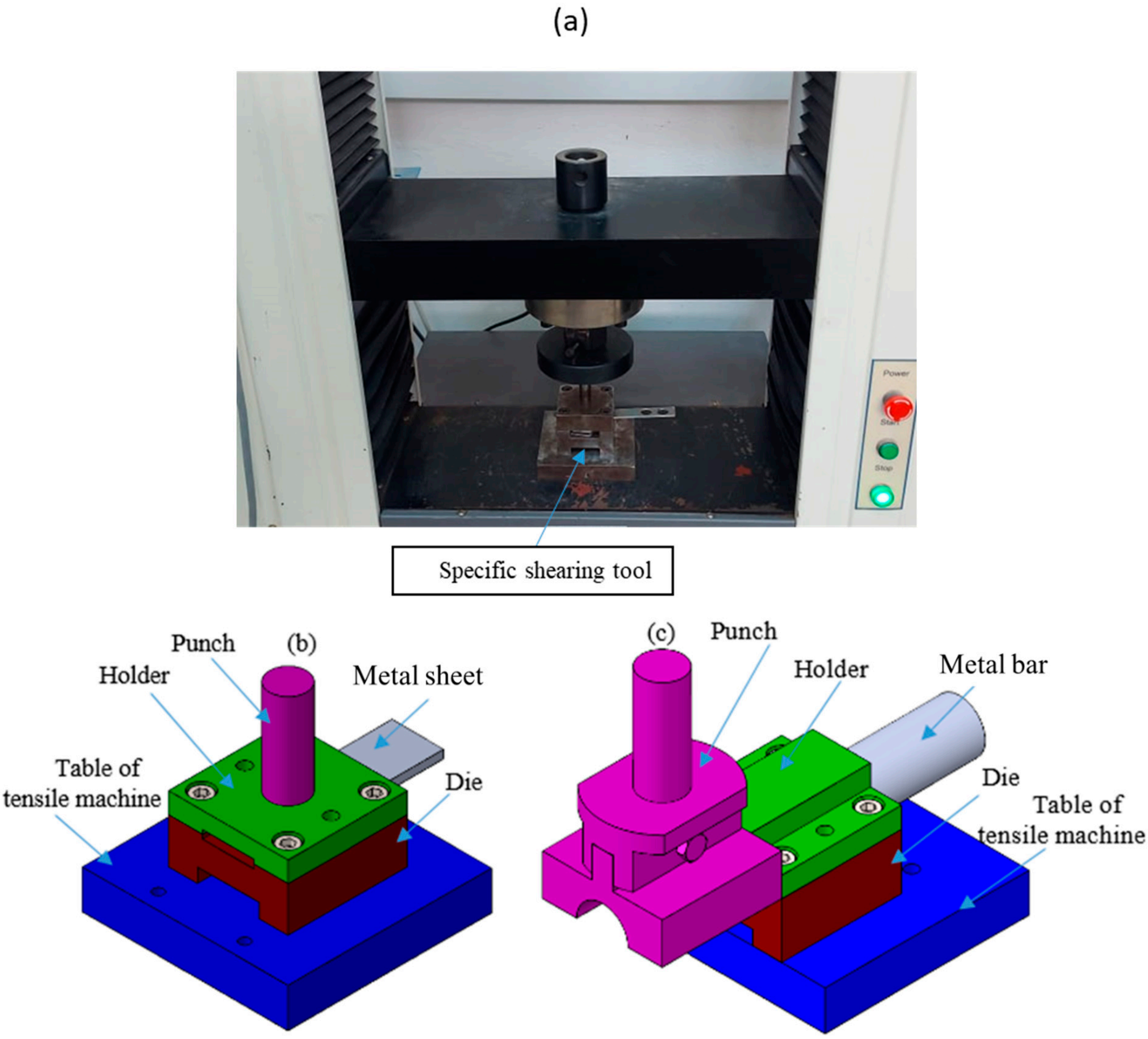

Figure 1. Experimental shear cutting tools: (**a**) tensile machine; (**b**) specific sheet shearing tool; (**c**) specific bar shearing tool.

Two grades of aluminium alloys are considered for the experimental and numerical tests. The first material is the 5083 aluminium sheet. Its thickness is 2 mm, and its elastic properties are illustrated in Table 1. The second material is the Al6061-T6 round bar. This aluminium bar has a diameter of 18 mm. Table 2 illustrates its thermomechanical properties.

Table 1. Elastic properties of 5083 aluminium sheet [24].

Yield Strength (MPa)	Poisson's Ratio	Young's Modulus (MPa)
106.3	0.33	75.6

Table 2. Al6061-T6 aluminium bar properties [25].

Density (g/cm^3)	Tensile Strength (MPa)	Yield Strength (MPa)	Young's Modulus (GPa)	Poisson's Ratio	Thermal Conductivity (W/mK)
2.7	310	275	69	0.33	167

3. Constitutive Models of Mechanical Behaviour and Damage

3.1. Governing True Stress–Strain Model

The true stress–strain equation is determined in order to set up a finite element simulation of the shear cutting operation. It is deduced from the engineering stress–strain curve, which is plotted by recording the engineering stress variation with the engineering strain until the bifurcation of the specimen. Both terms are known as nominal stress and nominal strain. The engineering stress–strain curve is obtained by progressively applying load F to a tensile test and measuring the engineering deformation (Equation (1)) from this experimental test. This curve reveals the mechanical properties of the workpiece.

$$\varepsilon = \frac{L - L_0}{L_0} \tag{1}$$

where L is the current length of the gauge section, and L_0 is the original length of the gauge section.

The engineering stress is calculated by dividing the applied load F by the original cross-section S_0. The nominal stress is given by Equation (2).

$$\sigma = \frac{F}{S_0} \tag{2}$$

However, the curve based on the instantaneous cross-section area S is called the true stress–strain curve. The instantaneous applied load divided by the instantaneous cross-sectional area of specimen S gives the true stress, as shown in Equation (3):

$$\sigma_v = \frac{F}{S} \tag{3}$$

For the true strain, Equation (4) gives the definition of this term:

$$d\varepsilon = \frac{dL}{L} \tag{4}$$

Both sides, which are given by Equation (4), are integrated, and the boundary conditions are applied. We obtain the following equation:

$$\varepsilon_v = \int_{L_0}^{L} \frac{dL}{L} \tag{5}$$

True strain is a logarithmic term. It is given by Equation (6):

$$\varepsilon_v = Ln\left(\frac{L}{L_0}\right) = Ln(1 + \varepsilon) \tag{6}$$

3.2. Empirical Formulations and Identification of Hardening Model

Good knowledge of the mechanical properties is needed in order to perform accurate numerical modelling of the manufacturing processes. Diverse empirical formulations have been proposed in order to predict the plastic deformation behaviour of materials in metal forming and cutting processes. One of the most commonly used formulations was proposed by Hollomon [26]. This power-law empirical relationship depends on two parameters: the strain-hardening coefficient and the strain-hardening exponent, respectively. Ludwik's law has an additional stress factor [27]. This model depends on three parameters, which are the yield strength, the coefficient of plastic resistance and the strain-hardening exponent. The Hollomon power law is not capable of describing the plastic behaviour at low strains for face-centred cubic steels with low stacking-fault energy (SFE). In fact, the stacking fault introduces an irregularity into the normal sequence of atoms. This irregularity carries the SFE. A modified Holloman relationship [28,29] was developed, which is extended to all metals regardless of the SFE. Two additional parameters are added in the modified Holloman law. In the same context, Swift [30] proposed a flow formulation by modifying the Holloman relationship. He takes into account a pre-strain term as a structural parameter.

Furthermore, when a workpiece is subjected to a high temperature as in forming and cutting processes, its strength tends to decrease. The thermal field has an effect on the evaluation of the flow stress model. In fact, in the shear cutting process, the temperature sensitivity should be taken into account when we define the plasticity and the damage laws. We define in these models the temperature sensitivity term $\underline{T}$, which is defined as shown in Equation (7). We denote T_0 and T_m as the reference and melting temperatures, respectively.

$$\underline{T} = \frac{T - T_0}{T_m - T_0} \tag{7}$$

Furthermore, an empirical plasticity law named the Johnson–Cook model (Equation (8)) was developed and is usually used to describe the ductile material's behaviour under strain hardening, strain rate hardening and thermal conditions [31].

$$\sigma_{eq} = \left(A + B\left(\varepsilon_{pl}\right)^{n}\right)\left(1 + C\,Ln\left(\underline{\dot{\varepsilon}}\right)\right)\left(1 - \left(\underline{T}\right)^{m}\right) \tag{8}$$

The constitutive parameters may be determined experimentally. In the current study, the reference temperature (Equation (7)) and the reference strain rate (Equation (9)) are taken, respectively, as 20° and 1 s^{-1}. In the flow stress model, we have

$$\underline{\dot{\varepsilon}} = \frac{\dot{\varepsilon}}{\dot{\varepsilon_0}} \tag{9}$$

The strain-hardening effect depends on three parameters, which are A, B and n. They are called the yield stress, flow stress and the strain-hardening coefficient, respectively. The strain rate strengthening effect depends on the strain rate coefficient, denoted as C. The last term represents the temperature effect. It contains the temperature dependence coefficient m. In our model of the shear cutting test, the strain rate's strengthening influence is neglected.

However, two laws are considered. In the first one, the temperature effect is not taken into account. The modified Johnson–Cook law is given by Equation (10).

$$\sigma_{eq} = \left(A + B\varepsilon_{pl}^{n}\right) \tag{10}$$

After rearranging Equation (10) and taking the logarithmic function on both sides of this law, a linear relationship between $Ln\left(\sigma_{eq} - A\right)$ and $Ln\left(\varepsilon_{pl}\right)$ was determined, as shown in Equation (11):

$$Ln\left(\sigma_{eq} - A\right) = n.Ln\left(\varepsilon_{pl}\right) + Ln(B) \tag{11}$$

This relationship is a linear function. Based on the experimental tensile test, the flow stress model given by Equation (10) is calibrated. Then, the strain-hardening parameters are predicted.

In the second law, the modified Johnson–Cook model is given by Equation (12):

$$\sigma_{eq} = \left(A + B\left(\varepsilon_{pl}\right)^{n}\right)\left(1 - \left(\underline{T}\right)^{m}\right) \tag{12}$$

In order to linearize this relationship, it is necessary to rearrange it, as follows, by considering the logarithmic function of the three terms:

$$Ln\left(1-\frac{\sigma_{eq}}{A+B\left(\varepsilon_{pl}\right)^{n}}\right)=m.Ln(\underline{T}) \tag{13}$$

After identification of the strain-hardening parameters (Equation (11) and fitting of the different data points, the temperature dependence coefficient m can be identified.

3.3. Constitutive Model of Ductile Damage

When the fracture initiation occurs in the workpiece, its strength property reduces during plastic deformation. The relationship between the damaged stress σ_D and the damage parameter D gives the damage evolution, as shown in Equation (14).

$$\sigma_D=(1-D)\sigma_{eq};\quad 0\leq D\leq 1 \tag{14}$$

The damage occurs when D reaches the maximum value D_{max} = 1.

Furthermore, numerical models take into account the influence of stress triaxiality η on the strain damage. The triaxiality factor is a dimensionless ratio between hydrostatic and Von Mises equivalent stresses. We denote σ_I, σ_{II} and σ_{III} as the principal tensor stresses. We then have

$$\eta=\frac{\sigma_m}{\sigma_{eq}}=\frac{\frac{\sigma_I+\sigma_{II}+\sigma_{III}}{3}}{\sqrt{\frac{1}{2}\left[(\sigma_I-\sigma_{II})^2+(\sigma_{II}-\sigma_{III})^2+(\sigma_{III}-\sigma_I)^2\right]}} \tag{15}$$

The triaxiality factor gives us an idea of the stress states in the sheared piece. Therefore, stress triaxiality is an important factor to consider in the design and analysis of ductile materials, particularly in high-stress and high-strain applications in which the risk of fracture is significant. By understanding the relationship between stress triaxiality and fracture behaviour, engineers can optimize the design of materials and structures to improve their strength, durability, and safety.

One of the damage models used in cutting processes is the Hooputra criterion [32]. It is widely used in the sheet shear cutting process, in which it assumes that the damage strain depends only on the triaxiality factor (Equation (16)).

$$\begin{gathered} D=\int\frac{\Delta\varepsilon_{pl}}{\varepsilon_f} \\ \varepsilon_f=a_1e^{a_3\eta}+a_2e^{-a_3\eta} \end{gathered} \tag{16}$$

where $\Delta\varepsilon$ is the equivalent plastic strain increment, and ε_f is the damage strain. The influence of the thermal term is not considered in this model. The material parameters, which are a_1, a_2 and a_3, should be identified experimentally. The maximal damage variable was fixed to D_{max} = 1. The failure happens when the damage variable reaches D_{max}.

Otherwise, as shown in Equation (17), the Johnson–Cook damage model describes the damage strain as a function of the stress triaxiality, strain rate and temperature fields.

$$\varepsilon_f=\left(D_1+D_2\,\mathrm{e}^{D_3\eta}\right)\left(1+D_4\,Ln\left(\underline{\dot{\varepsilon}}\right)\right)\left(1-D_5\underline{T}\right) \tag{17}$$

The damage material parameters (D_1 to D_5) are determined from experimental characterization tests. The cumulative damage parameter D is calculated as shown in Equation (18).

$$D=\sum\left(\frac{\Delta\varepsilon_{pl}}{\varepsilon_f}\right) \tag{18}$$

The modified Johnson–Cook law (Equation (19)) describes the fracture strain when the effect of strain rate is neglected. Only four parameters should be identified.

$$\varepsilon_f = \left(D_1 + D_2\, \mathrm{e}^{D_3\eta}\right)(1 - D_5\underline{T}) \tag{19}$$

When the effect of temperature is also neglected, the second modified Johnson–Cook law describes the fracture strain:

$$\varepsilon_f = \left(D_1 + D_2\, e^{D_3\eta}\right) \tag{20}$$

Both models (Equations (19) and (20)) will be used in numerical computations of shear cutting tests.

4. Variational Formulation of Shear Cutting Operations

Friction forces should be considered in any cutting process, mainly in machining and shear cutting tests. These forces play a critical role in the prediction of cutting parameters. In shear cutting operations, friction is mainly present between the workpiece and the tool. The contact force F_{fr} (Equation (21)) is decomposed into two parts, which are tangential and normal terms.

$$F_{fr} = F_{fr}^n + F_{fr}^t \tag{21}$$

The internal heat flux results only from the plastic strain and the contact friction between the workpiece and the shear cutting tools.

In addition, the fundamental governing equation of the dynamic system in continuum mechanics is given by Equation (22).

$$div(\underline{\sigma}) + f_d = \rho\ddot{U} \tag{22}$$

where $\underline{\sigma}$ is the symmetric stress tensor; it is defined with the behaviour law. f_d is the volume force, ρ is the mass density of workpiece, and $\ddot{U}$ is the acceleration. Based on the principle of virtual work, the total work done by the applied forces during a small virtual displacement δU is zero. This principle is shown in Equation (23):

$$W_{int} + W_{inert} = \sum W_{ext} \tag{23}$$

where W_{int} and W_{inert} are the internal and inertial virtual work, respectively. They are defined, respectively, by the following equations.

$$\begin{aligned} W_{int} &= \int_V \sigma\, \delta\dot{U}\, dV \\ W_{inert} &= \int_V \rho\, \ddot{U}\, \delta U\, dV \end{aligned} \tag{24}$$

In the same context, Equation (25) is the mathematical relationship of the external virtual work.

$$\sum W_{ext} = \int_V f_d\, \delta U\, dV + \int_{S_{fr}} \left(F_{fr}^n + F_{fr}^t\right) \delta U\, dS + \int_{S_\tau} \tau\, \delta U\, dS \tag{25}$$

where τ is the stress vector on the surface S_τ.

The variational form of the mechanical problem is given by the following equation:

$$\begin{gathered} \int_V \underline{\sigma} : \delta\underline{\varepsilon}\, dV + \int_V \rho\, \ddot{U}\, \delta\dot{U}\, dV \\ = \\ \int_V f_d\, \delta\dot{U}\, dV + \int_{S_{fr}} \left(F_{fr}^n + F_{fr}^t\right) \delta\dot{U}\, dS + \int_{S_\tau} \tau\, \delta U\, dS \end{gathered} \tag{26}$$

In addition, the thermal equation is given by Equation (27). C_v, T and k are the specific heat of the isotropic materials, the temperature rate and the thermal conductivity, respectively.

$$\rho\ C_v\ \dot{T} = div(k.grad(T)) + Q_{conv} + Q_{mec} \tag{27}$$

Q_{conv} is the work created by heat convection between the tools and the workpiece. Q_{mec} is generated by the mechanical contribution. It is given by Equation (28).

$$Q_{mec} = \eta_{pl}\ Q_{pl} + \eta_{fr}\ Q_{fr} \tag{28}$$

where η_p is the fraction of plastic work converted into heat Q_{pl}, η_{fr} is the fraction of friction work converted into heat in the workpiece Q_{fr}. The contact surface between the workpiece and the cutting tool is denoted S_f. The weak variational form of Equation (27) is expressed as follows:

$$\begin{gathered} \int_V \left(\rho C_p \dot{T} - k\Delta T - \eta_{pl}\ \underline{\sigma} : \dot{\underline{\varepsilon}}\right)\delta T dV \\ = \\ -\int_{S_{fr}} \left(\eta_{fr} f_{fr} \tau_{fr}\ \dot{U} + h(T - T_{tool})\right)\delta T dS \end{gathered} \tag{29}$$

The space of functions and their derivatives are L^2-integrable and belong to the H^1 space. We denote δT as an arbitrary temperature variation. T_{tool} is the temperature of the tool, and h is heat transfer coefficient due to thermal convection. Then, thermomechanical problem consists of solving the following system (Equation (30)).

$$\begin{cases} \int_V \left(\underline{\sigma} : \delta\underline{\varepsilon} + \rho\ \ddot{U}\ \delta\dot{U} - f_d\ \delta\dot{U}\right)dV = \int_{S_{fr}} \left(F^n_{fr} + F^t_{fr}\right)\delta\dot{U}\ dS + \int_{S_\tau} \tau\ \delta U\ dS \\ \int_V \left(\rho C_p \dot{T} - k\Delta T - \eta_{pl}\ \underline{\sigma} : \dot{\underline{\varepsilon}}\right)\delta T dV = -\int_{S_{fr}} \left(\eta_{fr} f_{fr} \tau_{fr}\ \dot{U} + h(T - T_{tool})\right)\delta T dS \end{cases} \tag{30}$$

Using the finite element method, the continuum mechanical problem described in Equation (30) is discretized, in which the total computation step is decomposed into a Δt time step (Appendix A).

After developing mathematical equations of thermomechanical shear cutting problem, numerical results will be presented in the next sections. The accuracy of the developed numerical models will be evaluated.

5. Numerical Models of Shear Cutting Operation

5.1. Numerical Model of Sheet Shear Cutting

The studied material is the 5083 aluminium alloy. A finite element code ABAQUS/Explicit is used in order to simulate the shear cutting operation of the 5083 aluminium sheet, which is meshed using a four-node bilinear axisymmetric quadrilateral element (CAX4R). In this section, the J2 yield criterion is used to describe the yielding behaviour of the aluminium material. As illustrated in Figure 2, we use a refined mesh in the failure zone. In our numerical model, the punch, the die and the holder are supposed rigid solids.

The diameters of the punch and die are 12 mm and 12.25 mm, respectively. The Coulomb friction model is used with a friction coefficient of 0.3. The parameters corresponding to the isotropic hardening are given in Table 3.

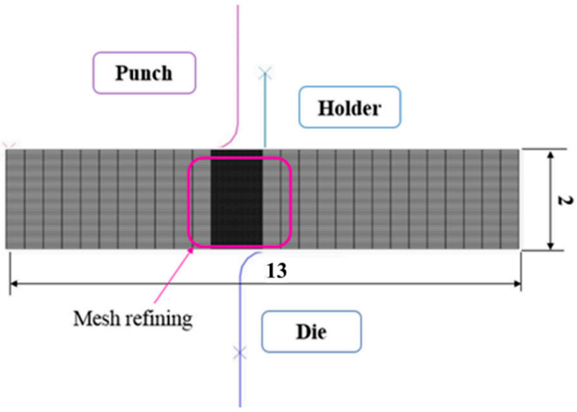

Figure 2. Numerical model of the sheet shear cutting operation.

Table 3. Behaviour parameters of 5083 aluminium sheet [24].

Young's modulus (MPa)	75,636
Poisson's ratio	0.33
Isotropic hardening parameters (MPa)	$\sigma\left(\varepsilon_{pl}\right) = 106.36 + 235.77\left(1 - e^{-9\ \varepsilon_{pl}}\right) + 54.36\left(1 - e^{-514\ \ \varepsilon_{pl}}\right)$

5.2. Numerical Model of Bar Shear Cutting

The bar shear cutting process is modelled in this section. Figure 3 shows the numerical model of this process. The bar is assumed to be composed of isotropic materials. Therefore, The J2 yield criterion, also known as the Von Mises yield criterion, is used for predicting the yield behaviour of the aluminium bar under complex stress states. In order to consider the element deletion method, the sample is fine-meshed in the shear zone. In fact, the element mesh size is 0.1 mm in this zone.

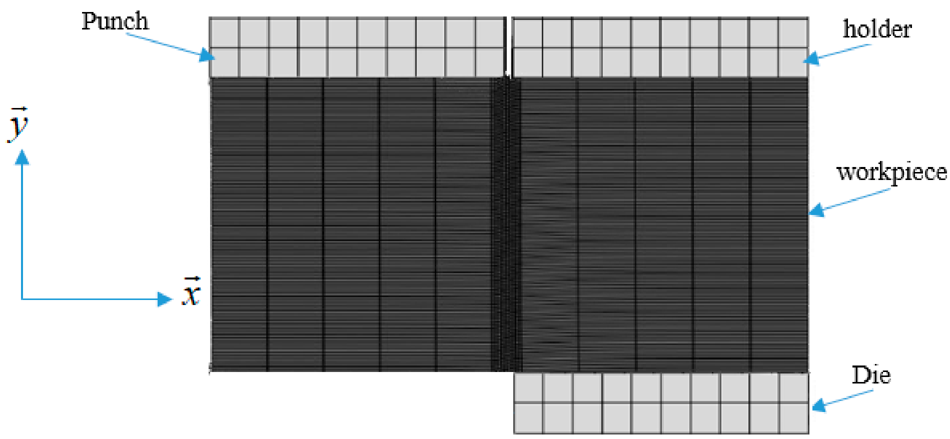

Figure 3. Moving and fixed parts of the shear cutting model.

All tools are considered rigid solids. The aluminium bar is modelled as an elastoplastic solid. The action applied by the punch on the bar causes a high shear deformation in the shear zone. The punch has a shear speed of V_{sh} = 200 mm/min. The holder and the die are clamped in this model. The Coulomb friction model is used with a friction coefficient of 0.3.

Experimental characterization tests are elaborated on the 6061-T6 aluminium bar by [33] in order to predict the Johnson–Cook parameters for the aluminium alloys. They are estimated as drawn in Table 4.

Table 4. Johnson–Cook parameters of Al6061-T6 aluminium bar [33].

A (MPa)	B (MPa)	n	m	D_1	D_2	D_3	D_5
250	79.7	0.5	1.5	−0.77	1.45	−0.47	1.6

The plasticity and damage mechanics are modelled with the modified Johnson–Cook model. For the bar shear cutting process simulations, two models are used. The first one considers only the mechanical behaviour and damage laws of the bar (Equations (10) and (19)). The second considers the thermal effect (Equations (12) and (20)) during the shear cutting process, which can significantly affect the flow stress and damage strain of the material.

For the mechanical model, the sheared workpiece is meshed with an eight-node linear brick element called C3D8 in Abaqus software. It is a fully integrated element. However, if we consider the thermomechanical model, the hexahedral thermally coupled elements with trilinear displacement and temperature (C3D8T) are used. In this model, four degrees of freedom are defined, which are three displacements in spatial directions with the temperature field.

6. Numerical Results and Discussion

6.1. Mechanical Model for Predicting Sheet Shear Cutting Operation

Mechanical models are used for the sheet metal in order to simulate the sheet shear cutting operation. In fact, Figure 4 illustrates the computed result.

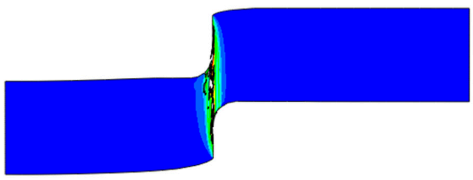

Figure 4. Numerical prediction of the sheet shear cutting operation for punch displacement of 1.1 mm.

Figure 5 illustrates a comparison between experimental and numerical curves. Figure 5 depicts the evolution of the shearing force vs. punch displacement during the shearing operation. It is notable that whether for the numerical or experimental results, a sudden drop in the shear force is detected, which is caused by a brutal crack propagation in the sheet metal. There is good correlation between the both curves, which proves the efficiency of the mechanical model in computing the sheet shear cutting operation.

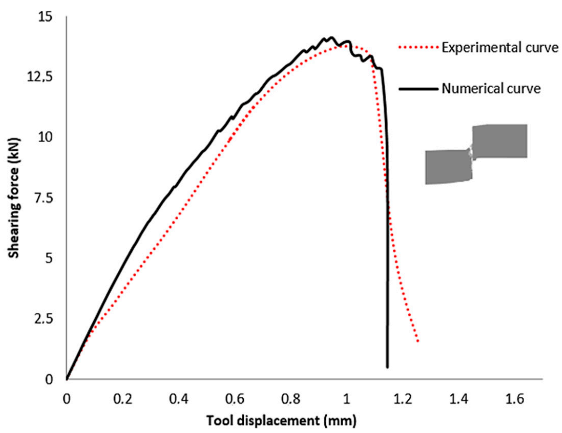

Figure 5. Sheet shear cutting tests: numerical and experimental results.

6.2. Thermomechanical Model for Predicting Bar Shear Cutting Operations

The bar shear cutting process of the Al6061-T6 alloy is simulated with the finite element code ABAQUS/Explicit. We denote with "Model 1" the modified Johnson–Cook plasticity and damage laws (Equations (10) and (19)), and with "Model 2" the modified Johnson–Cook laws (Equations (12) and (20)). Computed shearing force vs. tool displacement curves are illustrated in Figure 6.

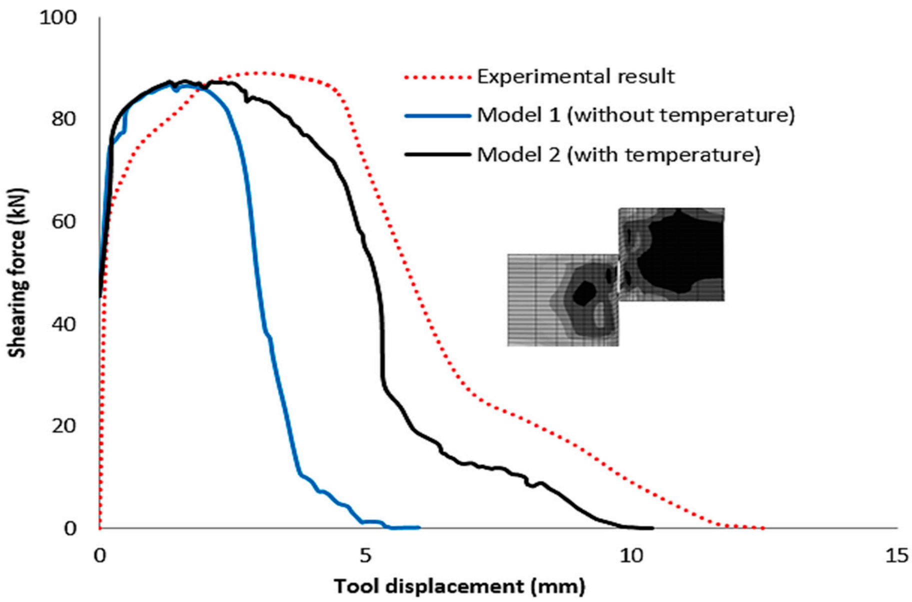

Figure 6. Bar shear cutting tests: numerical and experimental results.

The experimental shearing force was illustrated in the same Figure 6. During the experimental and numerical shear cutting operation, the clearance value is $c = 0.1$ mm.

The force–tool displacement curve contains four parts. The first is the elastic deformation. In this part, the curve evolution is linear. The second is the plastic deformation with hardening. If the curve attains the maximum value of shear cutting force, we obtain the plastic deformation with partial section reduction. Finally, macro crack nucleation and propagation are illustrated in the last zone. In Model 1, the temperature term is not considered in plasticity and damage relationships. This model incorrectly predicts the evolution of shearing force in the function of tool displacement. The numerical plastic deformation parts are smaller than the experimental parts, as shown in Figure 6. However, the maximum shear cutting force is approximately the same for both numerical models and for the experimental test. It has been noted in Figure 6 that using Model 2 gives a result very close to the experimental result. Finally, in the case of the bar shear cutting process, the temperature field should be considered in the constitutive behaviour of the aluminium material. This is because the shear cutting process can generate significant heat due to plastic deformation and friction between the cutting tool and the workpiece. The localized heating can affect the material's flow stress, damage accumulation, and microstructure evolution, leading to changes in the material's mechanical properties and potential failure modes.

A set of numerical tests of Model 2 are carried out in order to predict displacement (Figure 7) and temperature (Figure 8) fields that occur via shear cutting operations.

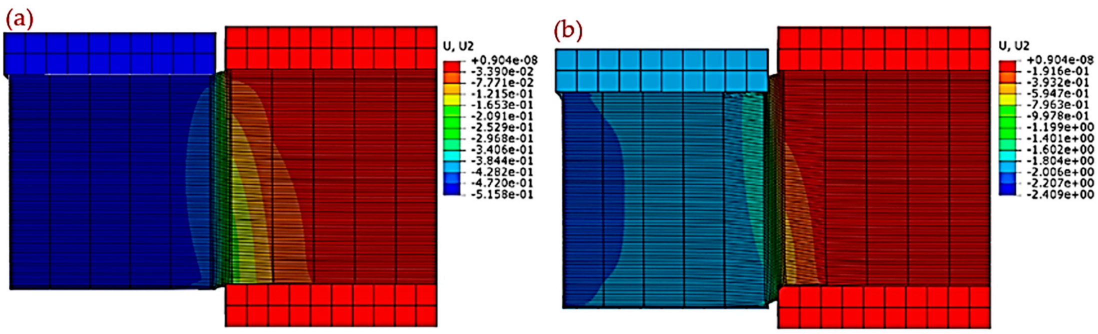

Figure 7. Displacement fields: (**a**) punch displacement U2 = 0.51 mm; (**b**) punch displacement U2 = 2.4 mm.

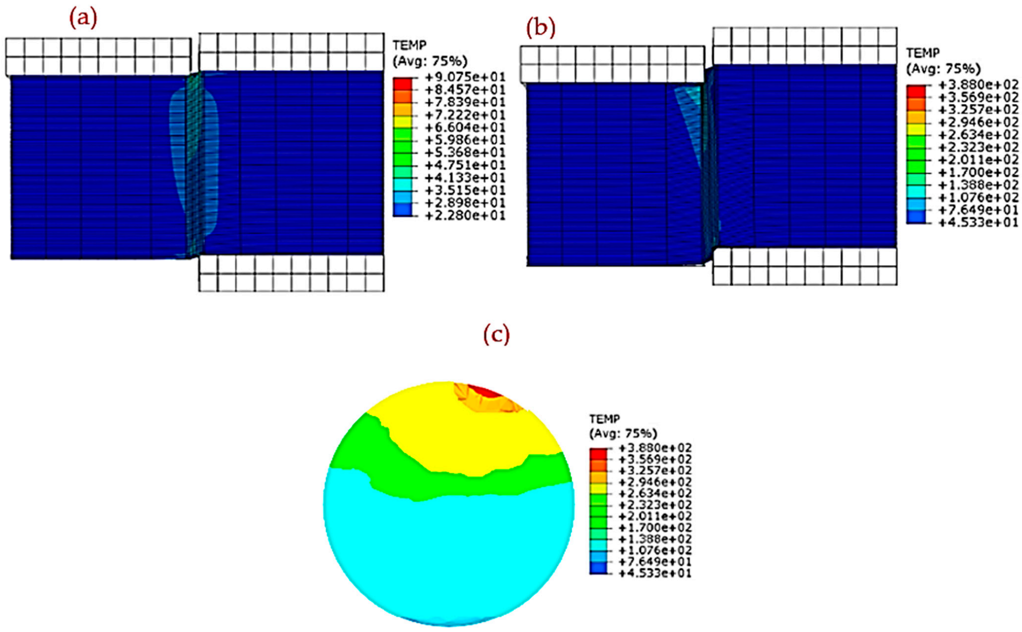

Figure 8. Temperature fields: (**a**) U2 = 0.51 mm; (**b**) U2 = 2.4 mm; (**c**) Temperature distribution on sheared surface (U2 = 2.4 mm).

The computed temperature fields in the bar metal show that the sheared surface reaches T = 90.7 °C with a punch displacement U2 = 0.51 mm (Figure 8a), and T = 388 °C with U2 = 2.4 mm (Figure 8b). The temperature distribution on the sheared surface with U2 = 2.4 mm is illustrated in Figure 8c. We deduce that the temperature increases significantly with the displacement of punch.

Friction work has a significant effect on the temperature fields in the bar workpiece generated during a shear cutting process. In fact, frictional forces are generated during the displacement of punch, which causes energy to be converted into heat. This explains the increase in temperature on the sheared surface. Therefore, this temperature, which is generated by friction, affects the mechanical properties of the bar workpiece.

In the shear cutting process, it is important to consider thermomechanical modelling that takes into account the temperature generated during cutting. This is because the temperature has a significant effect on the mechanical behaviour of the workpiece. This can lead to a more efficient and effective process of shear cutting bar metal. Thermomechanical modelling is used to predict the temperature distribution within the workpiece as well as the resulting deformation and stresses.

Figure 9 illustrates the damage evolution in workpiece. An element deletion method that eliminates the damaged element is applied to this model. This method allows a better simulation of the contact between the workpiece and the tools. An element is deleted from numerical model if the cumulative damage parameter reaches $D_{max} = 1$ at the integration points of the element. The output variables for this element are set to zero. In the next steps, the removed element has no energetic contribution to the shear cutting simulation.

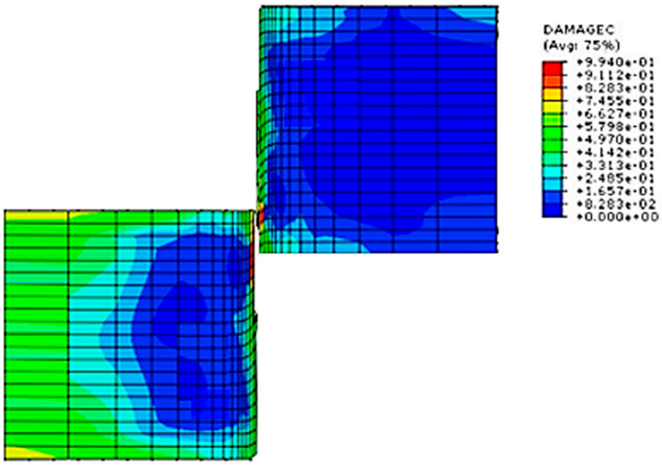

Figure 9. Damage fields.

6.3. Influence of Clearance on the Sheared Surface Quality

After proving the accuracy of Model 2 in predicting the shearing force and the ductile failure of the bar workpiece, a parametric analysis will be conducted in this section in order to determine the influence of clearance c, as a shear cutting parameter, on the sheared bar geometry. Three clearance values are chosen: $c_1 = 0.2$ mm, $c_2 = 0.5$ mm and $c_3 = 1.2$ mm. The most useful measures of sheared workpiece geometry are the burr (b) and the roughness of the sheared surface (a).

The computed burr created in the bar is analyzed. Figure 10 illustrates the final geometry of the workpiece.

Clearance	Geometry	Burr
$c_1 = 0.2 mm$	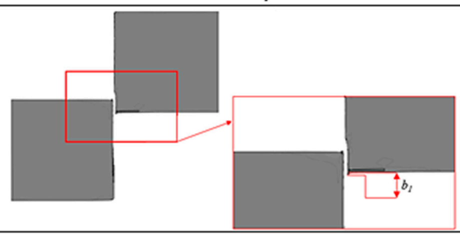	$b_1 = 0.4 mm$
$c_2 = 0.5 mm$	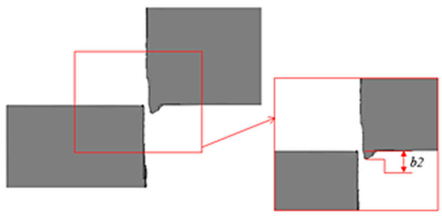	$b_2 = 1.2 mm$
$c_3 = 1.2 mm$	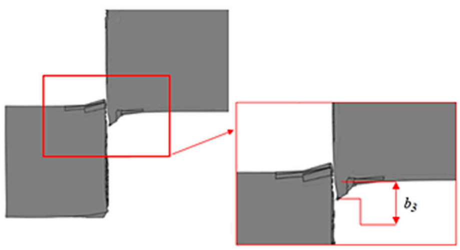	$b_3 = 2.1 mm$

Figure 10. Influence of shear clearance on the burr with $c_1 = 0.2$ mm, $c_2 = 0.5$ mm, and $c_3 = 1.2$ mm.

For the low shear clearance (c_1), the burr (b_1 = 0.4 mm) is small and the fractured zone is minimal. However, when the shear clearance increases (c_3), a larger fractured zone is obtained and the burr (b_3 = 2.1 mm) increases. We deduce from Figure 10 that the increase in the shear clearance causes a high burr value.

In the same context, the influence of shear clearance on the quality of the sheared surface is studied (Figure 11).

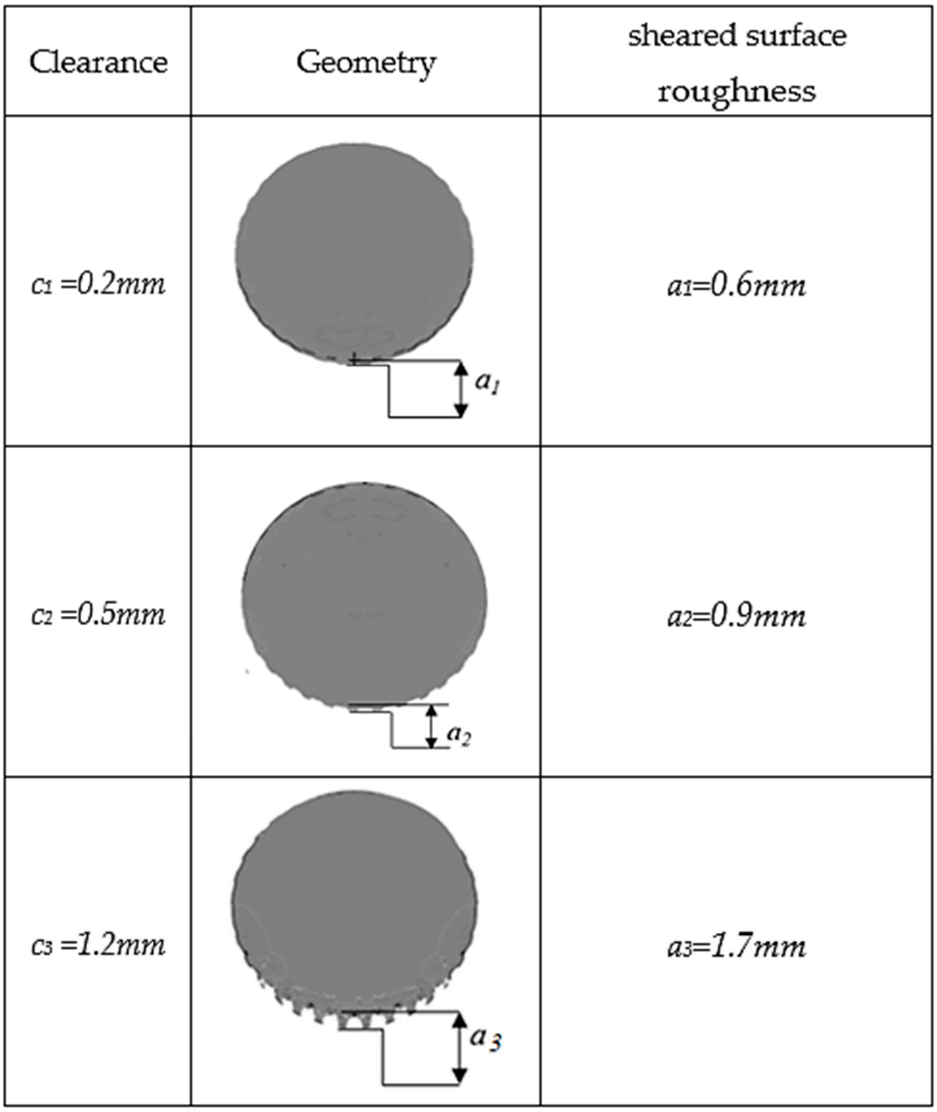

Figure 11. Influence of shear clearance on the sheared surface roughness with c_1 = 0.2 mm, c_2 = 0.5 mm, and c_3 = 1.2 mm.

With a low shear clearance (c_1), the best quality of sheared surface (a_1 = 0.6 mm) is obtained. However, with a high shear clearance value (c_3), a worse quality (a_3 = 1.7 mm) is found. As shown in Figure 11, the increase in the shear clearance causes the quality to worsen.

In summary, burrs are a common occurrence in the process of shear cutting metal, and their size and shape affect the roughness of the sheared surface. A good choice of shear cutting parameters can minimize the size of burrs and reduce the roughness of the sheared surface.

7. Conclusions

A mathematical formulation of the thermomechanical problem of the shear cutting process is developed. Various flow stress and damage models are analyzed. Modified Johnson–Cook hardening and damage models are used to describe the mechanical behaviour of aluminium materials, taking into account the temperature field generated during the bar shear cutting process.

Experimental and numerical force–displacement curves of the shear cutting process are presented for both sheet and bar. By comparing the numerical and experimental results of shearing force and tool displacement during both sheet and bar shear cutting operations, it was found that the use of a thermomechanical model was crucial in accurately predicting the mechanical behaviour of the aluminium alloys during bar shear cutting. The study found that the thermomechanical model was able to accurately predict the temperature distribution and strain during the bar shear cutting process. In contrast, the sheet shear cutting process was found to be less sensitive to the use of a thermomechanical model. This is likely due to the fact that the deformation during sheet shear cutting is more uniform and less localized than during bar shear cutting.

In addition, numerical parametric studies are conducted in order to predict the influence of the shear clearance on the geometrical defects of bar workpiece. The evolution of burr and the quality of the sheared surface for different values of clearance are observed. Specifically, it is found that as the shear clearance increases, the burr height increases and the quality of the sheared surface decreases. This is because larger clearance values result in a larger deformation zone, which can lead to more severe deformations and greater surface defects.

Finally, the shearing process can also affect the surface finish and cleanliness of the bar. Surface defects can be carried over into the forging process, potentially leading to surface defects or other quality issues in the final product. In a forthcoming publication, the influence of the shearing process on the forging process may be studied in detail.

Author Contributions: L.B.S.: Conceptualization, Methodology, experimental investigation, Writing—Original draft preparation, Review and Editing. A.K.C.: Software, visualization, Data curation, investigation. M.W.: Supervision, Conceptualization, Methodology, Writing—Review and Editing. All authors have read and agreed to the published version of the manuscript.

Funding: This research received no external funding.

Institutional Review Board Statement: Not applicable.

Informed Consent Statement: Not applicable.

Data Availability Statement: Not applicable.

Conflicts of Interest: The authors declare no conflict of interest.

Appendix A. Special Discretization of Thermomechanical Problem

In this Appendix, we describe the special discretization of the thermomechanical problem used in the paper. The FEM is used to discretize both the thermal and mechanical domains. The temperature distribution within the workpiece is approximated by solving the heat transfer equation within each element, while the deformation of the workpiece can be approximated by solving the momentum balance equation within each element. Using the finite element method, the continuum mechanical problem (Equation (30)) is discretized, in which the total computation step is decomposed into a Δt time step. The displacement field $u_j^k(x, y, z, t)$ and its time derivatives of each node k of the element j are given by Equation (A1).

$$\begin{gathered} u_j = \sum_k \beta^k u_j^k \ ; \ \dot{u}_j = \sum_k \beta^k \dot{u}_j^k \ ; \ \ddot{u}_j = \sum_k \beta^k \ddot{u}_j^k \\ \delta \dot{u}_j = \sum_k \beta^k \delta \dot{u}_j^k \end{gathered} \tag{A1}$$

where β^k is the shape function at the node k.

The relationship of the mechanical problem is given in Equation (A2).

$$\left(\left[M_j^{ki}\right]_j^i - \left\{G_j^k\right\} \right) \delta \dot{u}_j^k = 0 \tag{A2}$$

where $\left[M_j^{ki}\right]$ is the mass matrix of the element j, $\left\{G_j^k\right\}$ is the resultant force's vector at the node k of the element j, and $_j^i$ is the acceleration at the node i of the element j. We represent $[D_k]$ as a matrix, which relies the differential matrix developed in the thermomechanical problem with the shape function matrix. All vectors and matrices used for each element j of the mechanical equilibrium are given in Equation (A3).

$$\begin{gathered} \left\{G_j^k\right\} = \int\limits_{V_j} [D_k]^{tr} \underline{\sigma}\, dV + \int\limits_{S_j/S_\tau} \left[\beta^k\right]^{tr} \tau\, dS + \int\limits_{S_j/S_{fr}} \left[\beta^k\right]^{tr} F_{fr}\, dS \\ \left[M_j^{ki}\right] = \int_{V_j} \rho \left[\beta^k\right]^{tr} [\beta^i] dV \end{gathered} \tag{A3}$$

In a cutting operation, the contact forces F_{fr} (Equation (21)) between tools, which are the punch and the die, and the workpiece are decomposed into normal and tangential components.

The normal force is responsible for holding the workpiece in place and preventing it from moving away from the shear cutting tool. The tangential force is responsible for actually shearing the metal bar.

Therefore, based on the virtual work formula for this formulation, we obtain

$$\begin{gathered} \left(\sum_{j=1}^{n} \left(\left[M_j^{ki}\right] {}_j^i - \left(\int\limits_{S_{fr}} \left[\beta^k\right]^{tr} F_{fr}^n\, dS + \int\limits_{S_{fr}} \left[\beta^k\right]^{tr} F_{fr}^t\, dS + \int\limits_{S_\tau} \left[\beta^k\right]^{tr} \tau\, dS \right) \right) \right) \delta \dot{u}^k \\ = \\ -\sum_j \int\limits_V \left[D^k\right]^{tr} \underline{\sigma} dV \delta \dot{u}^k \end{gathered} \tag{A4}$$

If the influence of temperature fields is taken account on the strain expression, the strain field becomes

$$\varepsilon = \varepsilon_{el} + \varepsilon_{pl} + \varepsilon_{th} \tag{A5}$$

Equation (A6) illustrates the temperature variable of each node, symbolized by k of the element j.

$$T_j = \sum_k \beta_T^k T_j^k \ ; \ \dot{T}_j = \sum_k \beta_T^k \dot{T}_j^k \tag{A6}$$

where β_T^k is the shape function related to temperature field at the node k. For each node k of the element j, the semi-discrete thermal energy balance is illustrated in Equation (A7). Here, the capacitance matrix is represented by $\left[C_j^{ki}\right]$. In the same equation, $\left[H_{j/\mathrm{int}}^k\right]$ and $\left[H_{j/ext}^k\right]$ are the internal and external heat flux vectors, respectively.

$$\left(\left[C_j^{ki}\right] \dot{T}_j^i + \left[H_{j/\mathrm{int}}^k\right] \right) \delta T_j^k = \left[H_{j/ext}^k\right] \delta T_j^k \tag{A7}$$

We obtain the system Equation (A8):

$$\begin{gathered} \left[C_j^{ki}\right] = \int\limits_{V_j} \rho C_v \left[\beta_T^k\right]^{tr} [\beta_T^i] dV \\ \left[H_{j/\mathrm{int}}^k\right] = \int\limits_{V_j} [D_k]^{tr} k\, T [D_k] dV - \int\limits_{V_j} \left[\beta^k\right]^{tr} \eta_{pl}\, \underline{\sigma} : \underline{\varepsilon}\, dV - \int\limits_{S_f/S_j} \left[\beta^k\right]^{tr} Q_f\, dS \end{gathered} \tag{A8}$$

For all elements, the thermal semi-discrete equilibrium equality is given by Equation (A9).

$$\begin{gathered}\sum_j\left[\left(\int_{V_j}\rho C_v\left[\beta_T^k\right]^{tr}\left[\beta_T^i\right]dV\right)\dot{T}_j^i\right]\delta T_j^k\\+\sum_j\left[\left(\int_{V_j}[B]^{tr}k\,T[B]dV-\int_{V_j}[\phi]^{tr}\eta_p\,\underline{\sigma}:\underline{\varepsilon}\,dV-\int_{S_f/S_j}[\phi]^{tr}Q_f dS\right)\right]\delta T_j^k\\=\\\sum_j\left[H_{j/ext}^k\right]\delta T_j^k\end{gathered}\tag{A9}$$

References

1. Calamaz, M.; Limido, J.; Nouari, M.; Espinosa, C.; Coupard, D.; Salaün, M.; Girot, F.; Chieragatti, R. Toward a better understanding of tool wear effect through a comparison between experiments and SPH numerical modelling of machining hard materials. *Int. J. Refract. Met. Hard Mater.* **2009**, *27*, 595–604. [CrossRef]
2. Ben Said, L.; Wali, M. Accuracy of Variational Formulation to Model the Thermomechanical Problem and to Predict Failure in Metallic Materials. *Mathematics* **2022**, *10*, 3555. [CrossRef]
3. Ben Said, L.; Allouch, M.; Wali, M.; Dammak, F. Numerical Formulation of Anisotropic Elastoplastic Behavior Coupled with Damage Model in Forming Processes. *Mathematics* **2023**, *11*, 204. [CrossRef]
4. Benzerga, A.A.; Leblond, J.B.; Needleman, A.; Tvergaard, V. Ductile failure modeling. *Int. J. Fract.* **2016**, *201*, 29–80. [CrossRef]
5. Oyane, M.; Sato, T.; Okimoto, K.; Shima, S. Criteria for ductile fracture and their applications. *J. Mech. Work. Technol.* **1980**, *4*, 65–81. [CrossRef]
6. Lemaitre, J. Local approach of fracture. *Eng. Fract. Mech.* **1986**, *25*, 523–537. [CrossRef]
7. Rice, J.R.; Tracey, D.M. On the ductile enlargement of voids in triaxial stress fields. *J. Mech. Phys. Solids* **1969**, *17*, 201–217. [CrossRef]
8. Gurson, A.L. Continuum Theory of Ductile Rupture by Void Nucleation and Growth: Part I-Yield Criteria and Flow Rules for Porous Ductile Media. *J. Eng. Mater. Technol.* **1977**, *99*, 2–15. [CrossRef]
9. Johnson, G.R.; Cook, W.H. A constitutive model and data for metals subjected to large strains, high strain rates and high temperatures. In Proceedings of the 7th International Symposium on Ballistics, The Hague, The Netherlands, 19–21 April 1983; pp. 541–547.
10. Johnson, G.R.; Cook, W.H. Fracture characteristics of three metals subjected to various strains, strain rates, temperatures and pressures. *Eng. Fract. Mech.* **1985**, *21*, 31–48. [CrossRef]
11. Shen, X.; Zhang, D.; Yao, C.; Tan, L.; Li, X. Research on parameter identification of Johnson–Cook constitutive model for TC17 titanium alloy cutting simulation. *Mater. Today Commun.* **2022**, *31*, 103772. [CrossRef]
12. No, T.; Gomez, M.; Karandikar, J.; Heigel, J.; Copenhaver, R.; Schmitz, T. Propagation of Johnson-Cook flow stress model uncertainty to milling force uncertainty using finite element analysis and time domain simulation. *Procedia Manuf.* **2021**, *53*, 223–235. [CrossRef]
13. Murugesan, M.; Jung, D.W. Johnson Cook Material and Failure Model Parameters Estimation of AISI-1045 Medium Carbon Steel for Metal Forming Applications. *Materials* **2019**, *12*, 609. [CrossRef]
14. Patil, S.P.; Prajapati, K.G.; Jenkouk, V.; Olivier, H.; Markert, B. Experimental and Numerical Studies of Sheet Metal Forming with Damage Using Gas Detonation Process. *Metals* **2017**, *7*, 556. [CrossRef]
15. Li, M. Micromechanisms of deformation and fracture in shearing aluminum alloy sheet. *Int. J. Mech. Sci.* **2000**, *42*, 907–923. [CrossRef]
16. Feistle, M.; Koslow, I.; Krinninger, M.; Golle, R.; Volk, W. Reduction of Burr Formation for Conventional Shear Cutting of Boron-alloyed Sheets through Focused Heat Treatment. *Procedia CIRP* **2017**, *63*, 493–498. [CrossRef]
17. Gotoh, M.; Yamashita, M. A study of high-rate shearing of commercially pure aluminum sheet. *J. Mater. Process. Technol.* **2001**, *110*, 253–264. [CrossRef]
18. Behrens, B.A.; Lippold, L.; Knigge, J. Investigations of the shear behaviour of aluminium alloys. *Prod. Eng.* **2013**, *7*, 319–328. [CrossRef]
19. Hu, C.L.; Chen, L.Q.; Zhao, Z.; Li, J.W.; Li, Z.M. Study on the pre-shearing cropping process of steel bars. *Int. J. Adv. Manuf. Technol.* **2018**, *97*, 783–793. [CrossRef]
20. Rachik, M.; Roelandt, J.M.; Maillard, A. Some phenomenological and computational aspects of sheet metal blanking simulation. *J. Mater. Process. Technol.* **2002**, *128*, 256–265. [CrossRef]
21. Mao, H.; Zhou, F.; Liu, Y.; Hua, L. Numerical and experimental investigation of the discontinuous dot indenter in the fine-blanking process. *J. Manuf. Process.* **2016**, *24*, 90–99. [CrossRef]
22. Liu, Y.; Tang, B.; Hua, L.; Mao, H. Investigation of a novel modified die design for fine-blanking process to reduce the die-roll size. *J. Mater. Process. Technol.* **2018**, *260*, 30–37. [CrossRef]

23. Sachnik, P.; Hoque, S.E.; Volk, W. Burr-free cutting edges by notch-shear cutting. *J. Mater. Process. Technol.* **2017**, *249*, 229–245. [CrossRef]
24. Bouhamed, A.; Mars, J.; Jrad, H.; Wali, M.; Dammak, F. Experimental and numerical methodology to characterize 5083-aluminium behavior considering non-associated plasticity model coupled with isotropic ductile damage. *Int. J. Solids Struct.* **2021**, *229*, 111–139. [CrossRef]
25. Škrlec, A.; Klemenc, J. Estimating the Strain-Rate-Dependent Parameters of the Johnson-Cook Material Model Using Optimisation Algorithms Combined with a Response Surface. *Mathematics* **2020**, *8*, 1105. [CrossRef]
26. Hollomon, J.H. Tensile deformation. *Trans. Metall. Soc. AIME* **1945**, *162*, 268–290.
27. Palaparti, D.P.R.; Choudhary, B.K.; Samuel, E.I.; Srinivasan, V.S.; Mathew, M.D. Influence of strain rate and temperature on tensile stress–strain and work hardening behaviour of 9Cr–1Mo ferritic steel. *Mater. Sci. Eng. A* **2012**, *538*, 110–117. [CrossRef]
28. Ludwigson, D.C. Modified stress-strain relation for FCC metals and alloys. *Metall. Trans.* **1971**, *2*, 2825–2828. [CrossRef]
29. Samuel, K.G. Limitations of Hollomon and Ludwigson stress-strain relations in assessing the strain hardening parameters. *J. Phys. D Appl. Phys.* **2006**, *39*, 203–212. [CrossRef]
30. Swift, H.W. Plastic instability under plane stress. *J. Mech. Phys. Solids* **1952**, *1*, 1–18. [CrossRef]
31. Priest, J.; Ghadbeigi, H.; Ayvar-Soberanis, S.; Liljerehn, A.; Way, M. A modified Johnson-Cook constitutive model for improved thermal softening prediction of machining simulations in C45 steel. *Procedia CIRP* **2022**, *108*, 106–111. [CrossRef]
32. Hooputra, H.; Gese, H.; Dell, H.; Werner, H. A comprehensive failure model for crashworthiness simulation of aluminium extrusions. *Int. J. Crashworthiness* **2004**, *9*, 449–464. [CrossRef]
33. Sohail, A.; Syed Husain, I.; Jaffery, M.K.; Muhammad, F.; Aamir, M.; Liaqat, A. Numerical and experimental investigation of Johnson–Cook material models for aluminum (Al 6061-T6) alloy using orthogonal machining approach. *Adv. Mech. Eng.* **2018**, *10*, 1–14.